Climate sensitivity and cloud response of a GCM with a superparameterization

Matthew C. Wyant,[1] Marat Khairoutdinov,[2] and Christopher S. Bretherton[1]

[1] The climate sensitivity of an atmospheric GCM that uses a cloud-resolving model as a convective superparameterization is analyzed by comparing simulations with specified climatological sea surface temperature (SST) and with the SST increased by 2 K. The model has weaker climate sensitivity than most GCMs, but comparable climate sensitivity to recent aqua-planet simulations of a global cloud-resolving model. The weak sensitivity is primarily due to an increase in low cloud fraction and liquid water in tropical regions of moderate subsidence as well as substantial increases in high-latitude cloud fraction. **Citation:** Wyant, M. C., M. Khairoutdinov, and C. S. Bretherton (2006), Climate sensitivity and cloud response of a GCM with a superparameterization, *Geophys. Res. Lett.*, *33*, L06714, doi:10.1029/2005GL025464.

1. Introduction

[2] The sensitivity of the earth's climate to a warming perturbation is a problem frequently studied using general circulation models (GCMs). Unfortunately the responses of different GCMs to identical climate perturbations vary substantially, largely due to the differing response of modeled clouds to climate change [*Cess et al.*, 1989] (hereinafter referred to as C89). Cloud processes in conventional GCMs rely on parameterizations to represent motions smaller than the resolved grid scales and to calculate the fraction of the sky covered by cloud within each grid box.

[3] One potential alternative to GCMs is to directly resolve the atmosphere at a much finer resolution using cloud resolving models (CRMs). This permits explicit simulation of smaller-scale vertical convective motions associated with clouds. It also allows cloud fraction to be computed more naturally, and radiation to be calculated on a finer scale. Recently, the first climate perturbation simulations using a global CRM on an aqua planet were performed with the Nonhydrostatic Icosahedral Atmospheric Model (NICAM) [*Miura et al.*, 2005] with a horizontal resolution of 7 km. Because of the extremely large computational resources required, the climatology is based on 30 days of equinox simulation.

[4] Another recent approach, called superparameterization or Multi-Scale Modeling Framework (MMF) [*Grabowski*, 2001; *Khairoutdinov and Randall*, 2001; *Khairoutdinov et al.*, 2005, hereinafter referred to as K05] uses a two or three-dimensional CRM embedded in each column of a GCM to simulate small-scale convective circulations and associated clouds. The K05 model uses the System for Atmospheric Modeling (SAM) CRM [*Khairoutdinov and Randall*, 2003] embedded in the NCAR Community Atmospheric Model (CAM) GCM. This combined model, the SP-CAM, shows substantial improvement over CAM in simulating important aspects of the modern climate, including producing a realistic Madden-Julian oscillation and a more realistic diurnal cycle of convection over land (K05). At the same time it can produce much longer simulations than currently practical with a global CRM.

[5] Using SP-CAM, we present the first global atmospheric climate sensitivity experiments in a GCM with superparameterization. Following the approach of C89 and *Cess et al.* [1996] (hereinafter referred to as C96), we analyze the climate change as the SST is uniformly increased by 2 K.

2. Model Description and Experiment Setup

[6] SP-CAM, described in detail in K05, is based on the NCAR CAM which is the atmosphere component of the NCAR Community Climate System Model (CCSM) [*Blackmon et al.*, 2001]. A development version of CAM 3 with the semi-Lagrangian dynamical core is configured to run at T42 horizontal grid ($2.8° \times 2.8°$ spacing) with 30 levels (domain top at 3.6 hPa), and a time-step of 30 min. In each of the 8192 grid-columns of the MMF, the conventional moist-physics parameterizations including all cloud parameterizations are replaced with a CRM. The CRM also replaces CAM vertical diffusion and PBL parameterizations. Each CRM's fields are horizontally-uniformly forced by the large scale CAM fields, and the evolution of the horizontal-mean CRM fields, except for momentum, force the large scale CAM fields.

[7] The CRM is a two-dimensional version of SAM, which is described in detail by *Khairoutdinov and Randall* [2003]. The prognostic thermodynamic variables include the liquid/ice water moist static energy, the total non-precipitating water, and the total precipitating water. The mixing ratios of cloud water, cloud ice, rain, snow, and graupel are diagnosed from the prognostic variables using a partition between liquid and ice phases as a function of temperature. In this study, the CRM domain had 32 columns with 4-km horizontal grid spacing, 28 grid levels collocated and adjusted to follow CAM's grid levels, and a time-step of 20 s. The domain was aligned from north to south rather than from west to east as in the original SP-CAM used by K05. This was found to mitigate the precipitation bias in the Western Pacific for the summer months. The CAM radiative transfer scheme was applied every 15 min independently for each CRM column (in contrast to K05) with 0-or-1 cloud

---

[1]Department of Atmospheric Sciences, University of Washington, Seattle, Washington, USA.
[2]Department of Atmospheric Science, Colorado State University, Fort Collins, Colorado, USA.
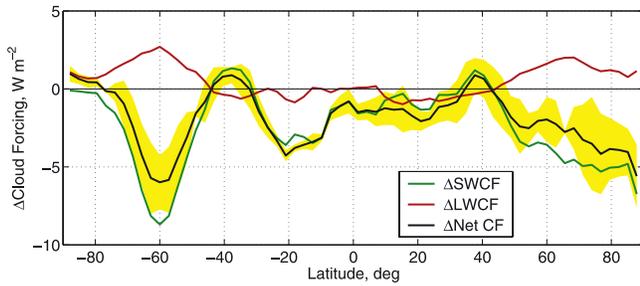
Figure 1. The annual zonal-mean changes in *SWCF* (green), *LWCF* (red), and net cloud forcing (black) of SP-CAM between the +2 K and control runs. The interannual standard deviation of the mean net cloud forcing change (see text) is plotted in yellow.

fraction for each grid point. The cloud fraction is computed using a condensate threshold of 0.01 times the local saturation mixing ratio.

[8] The control simulation was integrated starting on September 1st using the monthly-mean climatological sea-surface temperature (SST). The sea-ice climatology was also prescribed. The perturbation simulation is identical to the control except that the SST is uniformly increased by 2 K. The control simulation was run for 3.67 years and the +2 K simulation for 5.25 years, with the first 6 months considered as spin-up and therefore discarded from the analysis in each case.

3. Results

[9] Following C89, we calculate the climate sensitivity of the model by computing the change in top-of-atmosphere atmospheric radiative fluxes due to the imposed climate perturbation. The climate sensitivity parameter λ is defined by the equation

$$\Delta T_s = \lambda G, \qquad (1)$$

where ΔT_s is the global mean change in surface temperature and G is the change in global mean outgoing radiation. Using annual mean values for ΔT_s and G in SP-CAM, $\lambda = 0.41$ K W^{-1} m^2. We have performed similar +2 K perturbation experiments with CAM 3.0 with a semi-Lagrangian dynamical core, CAM 3.0 with an Eulerian dynamical core, and with the GFDL AM2.12b. These have λ's of 0.41, 0.54, and 0.65 respectively; SP-CAM is about as sensitive or less sensitive than these GCMs. In fact, SP-CAM has only slightly higher climate sensitivity than the least sensitive of the models presented in C89 (The C89 λ values are based on July simulations).

[10] As was the case in C89 and C96, the climate sensitivity of the SP-CAM model relative to other models can be largely explained by changes in cloud radiative forcing. The other primary processes that affect the climate sensitivity, i.e., the water-vapor, lapse rate, and ice-albedo feedbacks, vary less between models. The zonal mean relative humidity in SP-CAM, similar to the aforementioned GCMs, increases or decreases by less than 5% (RH) throughout the troposphere except near the tropopause. The SP-CAM clear sky sensitivity parameter (as defined in C89) $\lambda_c = 0.61$ K W^{-1}

m^2, as compared with 0.62, 0.66, and 0.64 for the semi-Lagrangian CAM, Eulerian CAM and GFDL models, respectively. Thus the clear sky differences among the models are not a primary factor in the λ differences.

[11] The global annual mean changes in shortwave cloud forcing (*SWCF*) and longwave cloud forcing (*LWCF*) and net cloud forcing for SP-CAM are −1.94 W m^{-2}, 0.17 W m^{-2}, and −1.77 W m^{-2}, respectively. The negative change in net cloud forcing increases G and makes λ smaller than it would be in the absence of cloud changes. Figure 1 shows the zonal-mean annual changes in shortwave, longwave, and net cloud radiative forcing caused by the +2 K perturbation (The interannual variability in mean net cloud forcing is plotted in yellow. This is computed by discarding the first six months of the two simulations, differencing their net cloud forcing averaged over each of the next three years, and estimating the standard deviation at each latitude from the variations between these three annual means.) Shortwave cloud forcing becomes more negative at all latitudes, except for narrow bands near 40N and 40S, indicating more cloud cover and/or thicker clouds at most latitudes. The change in zonal-mean longwave cloud forcing is relatively small and negative in the tropics and stronger and positive poleward of 40N and 40S, where it partly offsets the shortwave cloud forcing change. Thus the net cloud forcing change is negative at most latitudes, and it is of comparable size in the tropics and the extra-tropics. We first analyze the changes in cloud forcing in the tropics and then briefly consider the changes in the extra-tropics.

[12] In the tropics, which we define as the region from 30N to 30S, we sort monthly-mean climatologies of cloud fraction and cloud condensate with the pressure-velocity at 500 hPa, ω_{500}, in 10 hPa day^{-1} bins, following the method of *Bony et al.* [2004]. In this way we attempt to remove the effects of dynamic changes, associated with changes in the spatial and seasonal variation of ω_{500}, from the overall changes. Bony found that the tropics-wide changes of GCM cloud forcing due to dynamic changes were small compared to net changes averaged within ω_{500} bins. *Wyant et al.* [2006] further found that the tropics-wide total dynamic changes of most other cloud related variables were also small during climate perturbation experiments. Therefore, we will focus on cloud and cloud-forcing changes within ω_{500} bins.

[13] Figure 2 shows the ω_{500} changes in SP-CAM simulated *SWCF* and *LWCF* from 30S to 30N. The tropical reduction in net cloud forcing is primarily due to more negative *SWCF* in regimes of moderately strong monthly mean subsidence (20−30 hPa day^{-1}), and secondarily due to modest decreases in *SWCF* in other regions. The *LWCF* changes are slight in most ω_{500} regimes.

[14] We also applied tropical ω_{500}-sorting to GCM grid-box mean condensate (liquid water + ice) and to cloud fraction in the control run (Figure 3a) and to the bin-mean changes of these quantities (Figure 3b). The control run condensate fields show significant concentration of cloud condensate in the strong ascent regimes ($\omega_{500} < -20$ hPa day^{-1}) especially at low levels (from 700−900 hPa) with a secondary peak centered at 350 hPa, composed mostly of ice water. In subsiding regimes, the low cloud condensate between 850 and 950 hPa is also substantial, representing trade-cumulus and stratocumulus clouds. Cloud fraction is
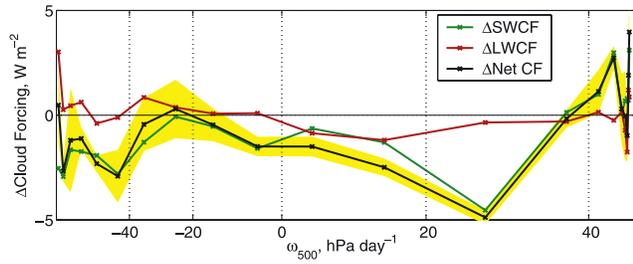
Figure 2. Changes in *SWCF* (green), *LWCF* (red), and net cloud forcing (black) sorted by ω_{500}-bin between the +2 K run the control run for 30S–30N. The x-axis is stretched proportional to ω_{500}-bin population. The interannual standard deviation of the mean net cloud forcing change is plotted in yellow.

Figure 3. (a) Control run and (b) changes with +2 K SST of cloud liquid-water + ice-water path and cloud fraction sorted by monthly mean ω_{500} for 30S–30N.

generally less than 0.1 at most heights and ω_{500} values, except for high cirrus and cirrostratus in strong ascent regions where the monthly mean cloud fraction can exceed 0.3. Lesser cirrus concentrations extend into the subsidence regimes. Mid-level clouds are largely confined to regions of strong ascent, while low level clouds have significant concentrations in both ascending and subsiding regimes.

[15] Figure 4 compares the tropical ISCCP cloud fraction with SP-CAM cloud fraction calculated with an ISCCP simulator. The cloud fraction is sorted by monthly ω_{500} and represents the sum of all ISCCP thickness categories. Cloud fraction is also shown for CAM3 and GFDL AM2.12b simulations, described by *Wyant et al.* [2006]. This comparison has been further refined to separate the ISCCP optical thickness categories and is provided as Figure S1[1]. SP-CAM better predicts the cloud fraction in most dynamic regimes and pressure levels than the two comparison GCMs. Surprisingly, this conclusion also holds for the subsidence regions dominated by boundary layer cloud, which is poorly resolved even in a CRM. Hence the SP-CAM is an attractive tool for examining global cloud responses to climate change.

[16] In the tropics there are substantial changes in both cirrus clouds and boundary-layer clouds in SP-CAM due to the +2 K SST change (Figure 3b). The cirrus clouds at the 150–350 hPa levels in ascent regions have the largest increases in area-averaged condensate, but a decrease in cloud fraction. These effects largely cancel each other radiatively. There is a substantial (>0.1) increase in cirrus cloud fraction at 100 hPa, but the condensate amounts at this level are too small to be radiatively significant. The boundary layer cloud condensate increases in most dynamical regimes, and particularly so in strong subsidence regimes (20–30 hPa day^{-1}), where the cloud fraction also increases. Both factors result in more negative *SWCF* with minimal additional *LWCF*. The net negative cloud radiative forcing changes in the tropics are dominated by these boundary layer cloud changes.

[17] The large negative cloud forcing in the extra-tropics (Figure 1) can be largely explained by broad increases in cloud fraction and cloud liquid water and ice path in SP-CAM. The changes in zonal-mean total condensate path
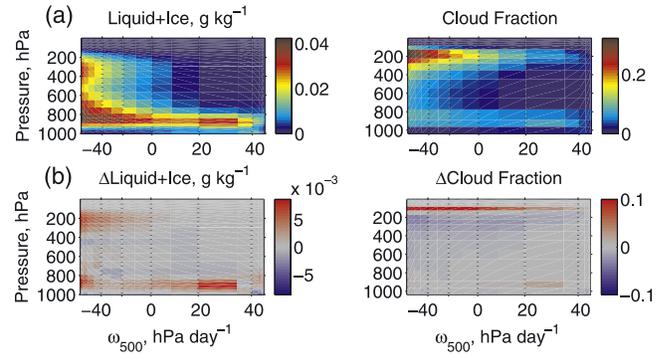
and column-integrated cloud fraction due to the +2 K SST rise are shown in Figure 5. (The column-integrated cloud fraction is based on a threshold condensate path of 0.02 kg m^{-2}.) The cloud condensate increases substantially poleward of 40 degrees, and column-integrated cloud fraction increases poleward of 50 degrees. The increases in cloud fraction and condensate cause *SWCF* to become more negative while *LWCF* only increases weakly, resulting in a net reduction of cloud forcing.

[18] The cloud fraction changes in Figure 5 are interesting to compare with the equinox based aqua-planet SST +2 K perturbation experiments of the NICAM global CRM [*Miura et al.*, 2005]. Poleward of 50 degrees, both models have strong cloud fraction increases despite their differing surface boundary conditions. In the subtropics and tropics the models don't agree as well. SP-CAM cloud fraction increases in ITCZ regions, while the NICAM cloud fraction decreases in the ITCZ. The climatically important increases in subtropical cloudiness in SP-CAM are weaker in NICAM. Despite these differences the NICAM simulations have a similar climate sensitivity parameter, $\lambda = 0.44$ K W^{-1} m^2.

[19] The annually averaged global mean surface precipitation in SP-CAM increases by 7.8% from 2.84 mm day^{-1}
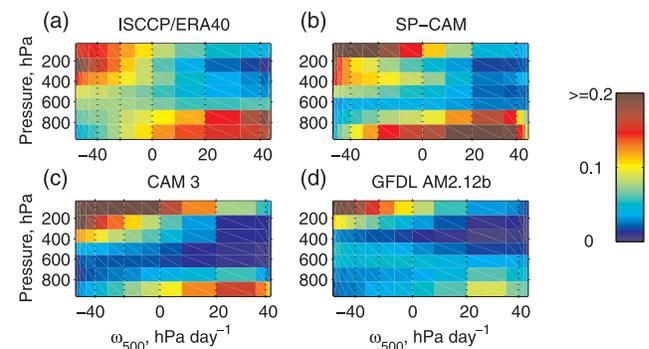
Figure 4. Comparison of (a) ISCCP cloud fraction for 30S–30N sorted by ECMWF ERA40 ω_{500} with ISCCP-simulator cloud fraction of (b) SP-CAM model climatology, (c) CAM 3 (Eulerian core) AMIP, and (d) GFDL AM2.12b AMIP simulations. The cloud fraction is summed over all optical thickness categories. Based on *Wyant et al.* [2006].

[1]Auxiliary material is available at ftp://ftp.agu.org/apend/gl/2005gl025464.
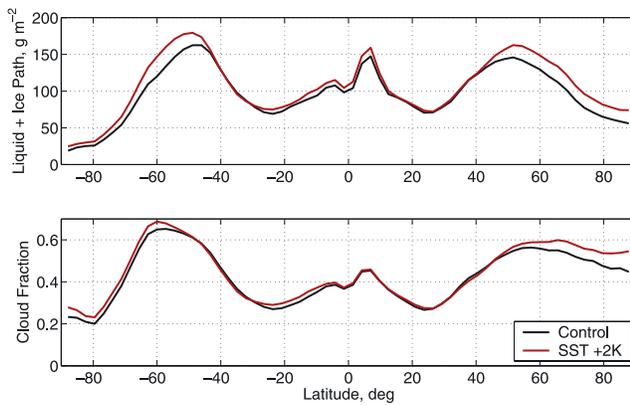
Figure 5. The annual zonal-mean changes in (top) liquid + ice path, g m^{-2} and (bottom) column-integrated cloud fraction for the control (black) and +2 K (red) runs.

to 3.07 mm day^{-1} due to the +2 K SST increase. This global increase is reflected in the entire annual cycle and is highly correlated with the control mean precipitation. The 30S−30N mean fractional increase is also 7.8% with increases of 15−20% in ITCZ regions, corresponding to a focusing of the rainfall belts. This contrasts with NICAM, where the rainfall diminishes by over 25% at the center of the ITCZ. In the tropics there are substantial regional variations in precipitation change, especially in the Indian Ocean. Decreases in precipitation over land between 10S and 30S are closely related to net increased subsidence there. Surface precipitation also increases substantially in the high-latitude storm tracks over the oceans.

4. Discussion and Conclusions

[20] We have presented the first climate sensitivity tests using superparameterization embedded within a conventional GCM. The overall climate sensitivity of SP-CAM for the Cess-type perturbation is relatively weak compared to other GCMs, but fairly similar to the climate sensitivity derived from limited duration aqua-planet simulations of the NICAM global CRM.

[21] This weak sensitivity of SP-CAM is associated with negative net cloud forcing changes in both the tropics and the extra-tropics. In the tropics these are primarily due to increases in low cloud fraction and condensate in regions of significant mean mid-tropospheric subsidence. In the extra-tropics these are caused by a general increase in cloud fraction in a broad range of heights, and a strong increase of cloud liquid water path in the lower troposphere.

[22] SP-CAM's major advantage over conventional GCMs is the ability to resolve cloud motions at a much finer scale, allowing deep convective processes and cloud fraction to be represented more naturally than standard GCM parameterizations allow. In addition to the advantages over CAM documented in K05, comparisons with other US GCMs have shown that the SP-CAM has more realistic cloud properties. Comparisons using an ISCCP-simulator show more realistic fractional cloudiness at most heights and optical thicknesses than the GCMs compared by *Wyant et al.* [2006]. SP-CAM reduces some of the common

shortcomings of GCM clouds such as under-prediction of middle-level cloud fraction and thin cloud fraction, though they are still present. These weaknesses are probably related to the coarseness of vertical resolution common to all these models. Also the SP-CAM generally under-predicts cloud fraction in subtropical stratocumulus regions (K05).

[23] *Bony and DuFresne* [2005] point out that the high degree of dependence of simulated climate feedback on low cloud response is a common feature of climate models, and conventional models diverge greatly in their low cloud responses. Clearly the representation of ubiquitous low clouds and small scale convection is still a weak point with current vertical resolution of SP-CAM, and low clouds produce a dominant part of the net global cloud forcing change predicted by the model. Thus the overall climate sensitivities produced by the model must be regarded with caution. A next step with SP-CAM is to couple it to a slab-ocean model so that cloud responses in more realistic climate change scenarios can be evaluated.

References

Blackmon, M. B., et al. (2001), The community climate system model, *Bull. Am. Meteorol. Soc.*, *82*, 2357−2376.

Bony, S., and J. Dufresne (2005), Marine boundary layer clouds at the heart of tropical cloud feedback uncertainties in climate models, *Geophys. Res. Lett.*, *32*, L20806, doi:10.1029/2005GL023851.

Bony, S., J.-L. Dufresne, H. Le Treut, J.-J. Morcrette, and C. Senior (2004), On dynamic and thermodynamic components of cloud changes, *Clim. Dyn.*, *22*, 71−86.

Cess, R. D., et al. (1989), Interpretation of cloud-climate feedback as produced by 14 atmospheric general circulation models, *Science*, *245*, 513−516.

Cess, R. D., et al. (1996), Cloud feedback in atmospheric general circulation models: An update, *J. Geophys. Res.*, *101*, 12,791−12,794.

Grabowski, W. (2001), Coupling cloud processes with the large-scale dynamics using the cloud-resolving convective parameterization (CRCP), *J. Atmos. Sci.*, *58*, 978−997.

Khairoutdinov, M. F., and D. A. Randall (2001), A cloud resolving model as a cloud parameterization in the NCAR community climate system model: Preliminary results, *Geophys. Res. Lett.*, *28*, 3617−3620.

Khairoutdinov, M. F., and D. A. Randall (2003), Cloud resolving modeling of the ARM summer 1997 IOP: Model formulation, results, uncertainties, and sensitivities, *J. Atmos. Sci.*, *60*, 607−625.

Khairoutdinov, M., D. Randall, and C. DeMott (2005), Simulations of the atmospheric general circulation using a cloud-resolving model as a super-parameterization of physical processes, *J. Atmos. Sci.*, *62*, 2136−2154.

Miura, H., H. Tomita, T. Nasuno, S. Iga, M. Satoh, and T. Matsuno (2005), A climate sensitivity test using a global cloud resolving model under an aqua planet condition, *Geophys. Res. Lett.*, *32*, L19717, doi:10.1029/2005GL023672.

Wyant, et al. (2006), A Comparison of low-latitude cloud properties and responses in AGCMs sorted into regimes using mid-tropospheric vertical velocity, *Clim. Dyn.*, in press.

───────────────
C. S. Bretherton and M. C. Wyant, Department of Atmospheric Sciences, University of Washington, 408 ATG Bldg., Box 351640, Seattle, WA 98195−1640, USA. (mwyant@atmos.washington.edu)

M. Khairoutdinov, Department of Atmospheric Science, Colorado State University, 200 West Lake Street, Fort Collins, CO 80523, USA.